

## Effect of Roughness in the Development of an Adverse Pressure Gradient Turbulent Boundary Layer

Donald A. Chao<sup>1,2</sup>, Luciano Castillo<sup>2</sup>, and Özden F. Turan<sup>3</sup>

<sup>1</sup>Department of Flight Test Engineering  
 Sikorsky Aircraft Corporation, Jupiter, FL 33478 USA

<sup>2</sup>Department of Mechanical, Aerospace and Nuclear Engineering  
 Rensselaer Polytechnic Institute, Troy, NY 12180 USA

<sup>3</sup>School of Architectural, Civil and Mechanical Engineering  
 Victoria University, Melbourne, Victoria, 8001 AUSTRALIA

### Abstract

An experimental study was conducted to examine the effect of surface roughness on the development of an adverse pressure gradient turbulent boundary layer. Hot-wire anemometry measurements were carried out using single and x-wire probes in the APG region of an open return type wind tunnel test section. The same experimental conditions (i.e.  $T_\infty$ ,  $U_{ref}$ , and  $C_p$ ) are maintained between the smooth,  $k^+ = 0$ , and rough,  $k^+ = 41-60$ , cases. Results indicate that the mean velocity deficit and Reynolds stress profiles tend to increase with surface roughness. These effects of roughness were successfully removed from the outer mean velocity profiles using the Zagarola and Smits scaling,  $U_\infty \delta^*/\delta$ . Using the integrated boundary layer equation, the skin friction was computed and showed a 58% increase due to the surface roughness effect. The effects of pressure gradient were found to be significant, of which, different profile trends with similar magnitudes were found for outer Reynolds normal stresses scaled with  $U_\infty$ .

### Introduction

The ability to accurately predict all turbulent flows could lead to improvements in design of fluid interactive components. An ongoing challenge is the understanding of turbulent boundary layers with respect to flow separation, mixing, and drag reduction, as they are of great value for engineers and scientists. More accurate models of component performance in industry could lead to fewer physical prototype iterations, which in turn could reduce the overall design cost. Up until now, little has been done with respect to rough-walled turbulent boundary layers subjected to an adverse pressure gradient (APG). Figure 1 illustrates a boundary layer subjected to different external conditions including roughness and pressure gradient.

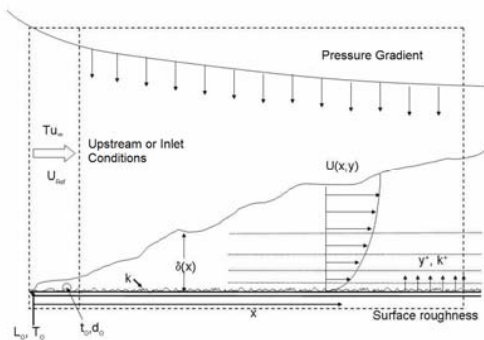


Figure 1. Schematic of external conditions of a boundary layer (Brzek [6])

The current experiment studies the effects of roughness in an APG flow, as it directly compares smooth and rough cases for an identical external APG flow configuration.

For a two-dimensional, incompressible, turbulent boundary layer, the Reynolds-averaged continuity equation is given in equation (1) below. The outer (typically  $y/\delta > 0.1$ ) and inner (typically  $y/\delta < 0.1$ ) x-component of the RANS (Reynolds-averaged Navier-Stokes equations reduce to equations (2) and (3), respectively,

$$\frac{\partial U}{\partial x} + \frac{\partial V}{\partial y} = 0, \quad (1)$$

$$U \frac{\partial U}{\partial x} + V \frac{\partial U}{\partial y} = \frac{-1}{\rho} \frac{\partial P_\infty}{\partial x} + \frac{\partial}{\partial y} \left[ -\langle uv \rangle + \nu \frac{\partial U}{\partial y} \right] + \frac{\partial}{\partial x} \left[ \langle v^2 \rangle - \langle u^2 \rangle \right], \quad (2)$$

$$0 = -\frac{1}{\rho} \frac{dP_\infty}{dx} + \frac{\partial}{\partial y} \left[ -\langle uv \rangle \right] + \nu \frac{\partial^2 U}{\partial x^2}, \quad (3)$$

imposing the no-slip condition at the wall  $U=0$  at  $y=0$ , and the boundary layer coinciding with the freestream velocity where  $U \rightarrow U_\infty$ .

The boundary layer is generally divided into two major regions, the inner and outer regions, where the viscous and inertial forces dominate, respectively. The inner region is from  $y^+ = 0$  to  $y^+ = 30$  and the outer region is from  $y^+ = 30$  to the edge of the boundary layer. If  $y^+ = 30$  is further from the surface than  $y/\delta = 0.1$  then there is no overlap region. This may occur when a flow encounters an increasingly large pressure gradient. The classical method of analyzing turbulent boundary layers consists of the law of the wall and the related logarithmic overlap law. Given that a flow may experience a non-existent overlap region, this classical method may erroneously describe the profile.

Flow separation characteristics in turbulent boundary layers are dependent on the APG being introduced. Ludwig and Tillmann [20] and Schubauer and Klebanoff [27] demonstrated that the skin friction coefficient,  $C_f$ , was reduced with adverse pressure gradients when compared to that of zero pressure gradients (ZPG). Clauser [15] also showed that even a gentle APG would half the skin friction coefficient compared to those of a constant pressure distribution with similar Reynolds numbers.

Bergstrom [5], Tachie et al. [30] and Tachie et al. [31] have demonstrated that the mean velocity profiles and Reynolds

stresses for ZPG flows have different characteristics between the smooth and rough surfaces and that roughness geometry plays an important role in the outer flow. Akinlade et al. [1] found similar results for the velocity profiles. According to Krogstad and Antonia [18], surface geometry significantly affects ZPG turbulent flow characteristics, turbulent energy production, and turbulent diffusion. Yet they found no difference in energy dissipation rate. Supporting this finding, was their  $uv$  quadrant analysis to show wall diffusion dependence on surface geometry. Krogstad and Antonia [19] support their previous work finding that the ZPG outer layer distributions of the Reynolds stress of two varying geometries are significantly different.

In terms of roughness, there are several variables that characterize roughness such as roughness element heights and their spacing. There have been a few tests performed on roughness with varying geometries such as wire meshes, rods, and sand paper, however data is lacking due to numerous geometry combinations. A few of these tests have been performed by Krogstad and Antonia [18] who have worked with wire meshes and lateral cylinder rods as roughness elements, Akinlade et al [1] who experimented with sand paper, perforated plates, and wire meshes, and Perry et al. [25] who machined out aluminum plates and timber for flush surface elements that were imbedded in the surface as opposed to protruding into the flow. This pool of roughness data has yet to find the key to intertwine these geometries as a single roughness parameter. Similar roughness heights, or  $k$  values can be used, but they do not incorporate element spacing. In general, a non-dimensional roughness parameter is used, which represents the ratio between the characteristic roughness height,  $k$ , and viscous length,  $u_*^*/\nu$ , defined as

$$k^+ = \frac{ku_*^*}{\nu}. \quad (4)$$

According to Schlichting [26], there are three roughness regimes in terms of  $k^+$ , hydraulically smooth, transitionally rough, and fully rough. When  $k^+ \geq 70$ , a flow is considered fully rough. The flow is considered hydraulically smooth for values of  $k^+$  between 0 and 5. For the regime in-between hydraulically smooth and fully rough there is a transitional regime. There is a definite need to classify these roughness regimes since these limits are sensitive to geometry and Reynolds number. Sand paper with varying grits has been one of the most ideal cases to study; yet a full analysis of all possible cases with one type of sand paper is to be established.

Furthermore, minimal attention has been given to rough-walled APG turbulent boundary layers. Perry et al. [25] are one of the few that have conducted investigations in this specific area. They introduced two types of roughness behaviors, 'k' and 'd' type roughness, and compared them within ZPG and APG flows. The 'k' type is defined as a flow where eddies induced by the roughness shed into the flow above the roughness elements, where elements are spaced relatively far apart with respect to element height. For this type, far enough off the surface, the roughness sublayer blends smoothly into the flow described by the velocity defect law. In a 'd' type surface the roughness elements are more closely spaced, where stable vortices within the grooves are apparent and there is minimal eddy shedding into the flow above the elements. In comparison to the 'k' type, 'd' type's outer flow travels relatively undisturbed over the roughness elements. For the APG cases, Perry et al. [25] used embedded pressure taps across the top of the roughness elements to formulate the skin friction coefficient. Results of the pressure readings indicated a monotonic decrease in skin friction down the plate.

From the available information and publications, it is evident that there is a lack of understanding of turbulent boundary layer flows, in particular, flows over rough surfaces subjected to an APG. These uncertainties have lead to some controversies, with no real distinguished solutions. Although there are encountered complexities, each test and result brings about a further understanding of individual scenarios, therefore all efforts are in the direction of progress.

### Skin Friction

One of the main goals in boundary layer research is determining the wall shear stress,  $\tau_w$ , the friction velocity,  $u_*^*$  and corresponding skin friction coefficient,  $C_f$ . The direct association with viscous drag, scaling parameters, and its effects in industry bring about a high emphasis on skin friction. Accurate calculations of skin friction can help predict drag forces, which in turn can aid the production of better fluid interactive components. Skin friction is also found to be critical for determining analytical parameters such as the similarity length scale  $y^+ = yu_*^*/\nu$ , Reynolds number  $\delta^+ = \delta u_*^*/\nu$ , and roughness parameter  $k^+ = ku_*^*/\nu$ .

This investigation utilized the integrated boundary layer equation in order to determine skin friction. After integrating the x-momentum equation (2) for a boundary layer from  $y'=0$  to  $y'=y$ , implementing the boundary conditions at  $y=0$ , and using the continuity and y-momentum equations, the integrated streamwise momentum equation is expressed as:

$$\frac{\tau_w}{\rho} = u_*^2 = \underbrace{\nu \frac{\partial \bar{U}}{\partial y}}_1 - \underbrace{\langle uv \rangle}_2 - \underbrace{\int_0^y \frac{\partial \bar{U}^2}{\partial x} dy'}_3 + \bar{U} \underbrace{\int_0^y \frac{\partial \bar{U}}{\partial x} dy'}_4 - \underbrace{\int_0^y \frac{\partial \langle u^2 \rangle}{\partial x} dy'}_4 + \underbrace{\int_0^y \frac{\partial \langle v^2 \rangle}{\partial x} dy'}_5 + \underbrace{U_\infty \frac{dU_\infty}{dx}}_6 y, \quad (5)$$

$V$  has been replaced by the continuity equation and with the use of Euler's equation the final term is in terms of freestream velocity,  $U_\infty$ , instead of the pressure gradient,  $dP_\infty/dx$ . The concept behind this method is that the shear stress on the left hand side of equation (5) remains constant throughout the entire boundary layer, causing the right hand side at any given y-location to be constant as well. This relationship leads to the determination of the wall shear stress and corresponding friction for smooth, rough and pressure gradient flows. Accuracy of this method, which was proven to be high by Newhall [22], depends highly on the spatial resolution of data in the streamwise direction for proper accounting of x-dependence. Other necessary requirements are the accurate measurement of the Reynolds stresses and that the flow be two-dimensional.

When analyzing the inner variables (below  $0.1\delta^+$ ), terms 3, 4, and 5 become negligible as the wall is approached reducing equation. (5) to:

$$\frac{\tau_w}{\rho} = u_*^2 = \underbrace{\nu \frac{\partial \bar{U}}{\partial y}}_1 - \underbrace{\langle uv \rangle}_2 - \underbrace{\frac{y}{\rho} \frac{dP_\infty}{dx}}_6. \quad (6)$$

At a distance of  $y^+ \geq 30$  from the wall and still within the inner region, the viscous stress (term 1) becomes negligible, which further reducing the equation to:

$$\frac{\tau_w}{\rho} = u_*^2 = -\underbrace{\langle uv \rangle}_2 - \underbrace{\frac{y}{\rho} \frac{dP_\infty}{dx}}_6, \quad (7)$$

Equation (7) allows for the direct computation of  $u_*^*$  from terms 2 and 6. When analyzing the current rough APG x-wire data (Flow

C), it was found that equation (7) did not hold true, since there was a finite contribution from the convection term, term 3. This contribution of term 3 was found to be as much as 6% in the inner region. Therefore the following equation was used to calculate  $u_*$  for x-wire Flow C data,

$$\frac{\tau_w}{\rho} = u_*^2 = \underbrace{-\langle uv \rangle}_2 - \underbrace{\int_0^y \frac{\partial \bar{U}^2}{\partial x} dy' + \bar{U} \int_0^y \frac{\partial \bar{U}}{\partial x} dy'}_3 - \underbrace{\frac{y}{\rho} \frac{dP_\infty}{dx}}_6 \quad (8)$$

Based on the error in the calculations of terms 3 and 6 (varying curve fitting schemes) from equation (8), and the measurement error in term 2, direct result percent errors and standard deviations of equation (8) for a given y-location are given in the following Table:

Parameter	Sigma, $\sigma$	% error
$u_*$	0.033	6.7
$C_f$	0.000154	8.7

Table 1. Friction velocity and friction coefficient error in the use of the Integrated Boundary Equation (inner region) for Flow C

The qualitative comparisons of  $C_f$  values for smooth data (Flow B) from Brzek [6] and Chao [13] and the new rough data acquired for this investigation (Flow C) are illustrated in Figure 2. The impact that roughness has on skin friction is clear. There is as much as a 28% increase in  $u_*$  and a 58% increase in  $C_f$  for Flow C. The pressure gradient effect is also apparent as the decreasing APG begins to negate the roughness effects, nearly merging the skin friction values for Flows B and C, at the end of the test section.

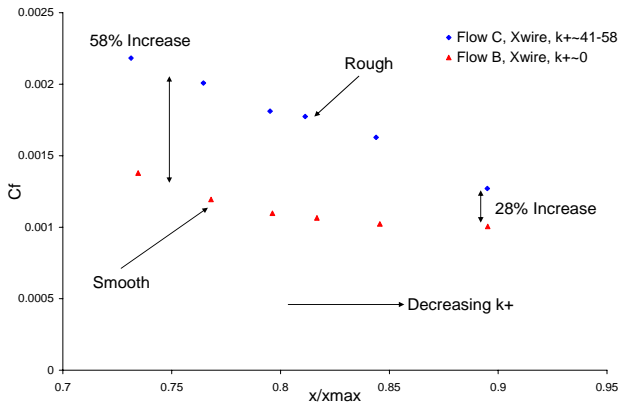


Figure 2. Friction coefficient  $C_f$  for Flows B and C in the APG region

### Scaling Techniques

As mentioned earlier, in general, the boundary layer is divided into the inner, overlap, and outer regions. Early investigations believed that a single scaling could depict the entire boundary layer, whereas the present beliefs lead to each region having its own scaling of the appropriate variables. The following subsections outline the Classical, Castillo and George [11], and Zagarola and Smits scaling [35].

### Classical Scaling

The theory behind the classical scaling is that in equilibrium turbulent boundary layers, both the inner and outer scales produce a single velocity scale,  $u_*$ . Clauser defines an

equilibrium turbulent boundary layer as one that satisfies the following,

$$\beta \equiv -\frac{\delta^*}{\rho u_*^2} \frac{dP_\infty}{dx} = constant \quad (9)$$

$$\frac{U_\infty - U}{u_*} = f(\bar{y}) \quad (10)$$

where the normalized velocity deficit profiles are independent of streamwise location even in rough pressure gradient boundary layers. The belief of this scaling is that the  $u_*$  scaling parameter collapses both the inner and outer variables of the boundary layer, where the hypothesis of single scaling must be satisfied. Clauser's criterion for equilibrium turbulent boundary layers was found to be satisfied by extremely controlled experiments, ones that are rarely found in nature, if found at all.

### Castillo and George Scaling

This scaling utilizes similarity analysis to evaluate the Reynolds-Averaged Navier-Stokes (RANS) equations to scale the velocity profiles and Reynolds stresses of turbulent boundary layers. George and Castillo [16] implemented this for smooth ZPG, while Seo [29] and Castillo et al [12] did it for rough surfaces. Castillo and George [11] did the same for flows exposed to external pressure gradients.

This analysis resulted in the scaling of the velocity profiles with the freestream velocity,  $U_\infty$ , the Reynolds normal stresses with  $U_\infty^2$ , and the Reynolds shear stress with  $U_\infty^2 d\delta/dx$ , where  $d\delta/dx$  is the boundary layer growth rate.

Furthermore, for equilibrium similarity conditions, George [17] suggests all the terms in the governing equations must remain balanced as the flow develops. Along with these constraints the pressure gradient parameter  $\Lambda$ , must remain constant as found in Castillo and George [1],

$$\Lambda \equiv -\frac{\delta}{U_\infty} \frac{dU_\infty}{dx} = constant \quad (11)$$

With this in mind, it was found that three distinct values of  $\Lambda$  can be obtained for the three different pressure gradient flows, where for APG  $\Lambda=0.22$ , for ZPG  $\Lambda=0$ , and for FPG  $\Lambda=-1.92$  (Castillo and George [1]).

### Zagarola and Smits Scaling

Zagarola and Smits [35] provided a new scaling,  $U_\infty \delta^*/\delta$ , for pipe and channel flow, which was developed empirically. Zagarola and Smits [34] implemented this scaling, collapsing on one curve the velocity profiles of a smooth surface ZPG turbulent boundary layer.

Walker and Castillo [32] showed that there are three distinct pressure gradient profiles (ZPG, FPG, and APG) when employing the Zagarola and Smits scaling for the mean velocity deficit profiles, Figure 3. These three distinct profiles are consistent with the behavior of pressure gradient parameter  $\Lambda$  described by Castillo and George [11]. Using this criterion, it was shown that the developing smooth APG flows, Flows A and B, exhibited developed APG behavior downstream of the initial start of the tunnel's APG region. This region of APG behavior described as the 'Full APG Region' (Anderson et al. [3] and [4] and Brzek [6]).

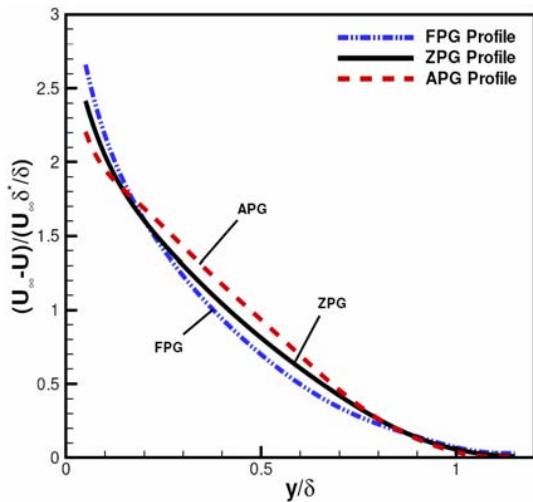


Figure 3. Zagarola and Smits average profiles of the three distinct pressure gradient bands as described by Walker and Castillo [32]. Profile averaging performed by Brzek [6].

### Experimental Setup

All calibrations and wind tunnel testing were performed in the Wind Tunnel Research Facility at Victoria University in Melbourne, Australia. This facility is comprised of an open return type wind tunnel with a 0.9 m by 0.9 m by 4.5 m long test section and a corresponding fully developed pipe flow apparatus for calibration and validation purposes. The test section was equipped with a flexible top for the production of varying pressure gradients. The pressure distribution used throughout (smooth and rough) this investigation is shown in Figure 4, where the 4% discrepancy smooth and rough cases can be attributed to experimental scatter.

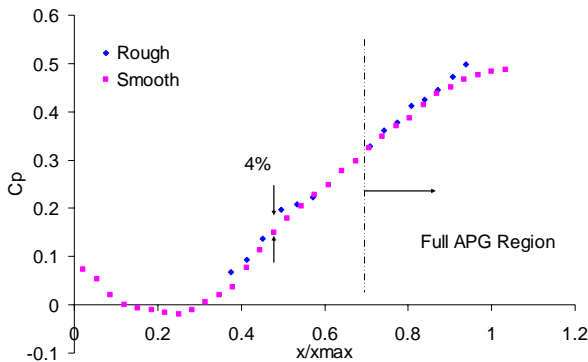


Figure 4.  $C_p$  distribution for smooth and rough cases in current investigation

In order to directly compare the features of the smooth APG data from Flow B (Anderson [2], Brzek [6], and Chao [13]) to the current roughness experiment, the same wind tunnel facility and identical configurations were utilized. Therefore Flow C, the current roughness experiment, is the rough implementation of Flow B. To employ roughness in the wind tunnel setup, a 24-grit abrasive sheet was attached to the false floor of the test section. A constant reference velocity of 22 m/s was maintained throughout the experiment.

Analyzed boundary layer characteristics were measured using hot-wire anemometry for six downstream locations in the full APG region. The anemometry hardware consisted of Dantec 55P05 single wire probes (boundary layer type), 55R51 x-wire probes, and a Streamline CTA system with collaborating Streamware software. Throughout single wire probe testing, the sampling frequency was set to 100 kHz to take 524,288 samples

(maximum number of samples possible) per traverse location, which translates to 5.24 seconds of data logging. The acquisition configuration for x-wire testing was set to a sampling frequency of 10 kHz to take 262,144 samples per wire (max number of samples), which translates to 26.2 seconds of data logging. Calibration of the single wire probes was conducted in a fully developed pipe flow apparatus. A calibrated look up table was created based on pressure drop and exit velocity relationships of the pipe apparatus. Calibration for the x-wire probe was performed in the wind tunnel and validated with comparisons to single wire measurements. The current experiment followed Lueptow [21] for the calibration procedure and look-up table creation for the x-wire probe. To gather the data for calibration, the x-wire probe was pitched through angles from  $30^\circ$  to  $-30^\circ$  relative to the streamwise direction within the free stream of the wind tunnel flow. Simultaneous measurements of both sensors of the probe were taken through the pitching and velocity varying of the procedure. For any given angle the probe was fixed in place, while the tunnel flow speeds were varied. At the location of the probe, velocities were varied from 4.8 m/s to 35 m/s. The result of the data set from the pitching procedure is a unique voltage pair  $(E_1, E_2)$  for a given pitch angle,  $\gamma$ , and velocity,  $Q$ . These angles and velocities are converted to velocity components,  $U=Q\cos(\chi)$  and  $V=Q\sin(\chi)$ , with respect to the probe orientation and geometry. This conversion of angles and velocities is what provided the matrix for the look-up table.

The percent errors in measurements for this investigation based on repeatability are presented in Table 2: The x-wire measurements tend to have a lower percent error since their logging times are longer providing better averaged values.

Variables	Single-wire		X-wire	
	Inner	Outer	Inner	Outer
$U$	6%	3%	4%	2%
$u^2$	7%	4%	5%	5%
$v^2$	-	-	4%	2%
$uv$	-	-	5%	3%

Table 2. Percent errors of single- and x-wire measurements based on repeatability for the inner and outer regions of the boundary layer.

### Results and Discussion

The following discusses results of smooth and rough wall turbulent boundary layers subjected to an APG. These comparisons use smooth data (Flow B) from Brzek [6] and Chao [13] and the new rough data acquired for this investigation (Flow C), all of which were measured using the same facility, wind tunnel configuration, and reference velocity (22 m/s). The flow is found to be in the transitionally rough regime ( $k^+ \sim 41-60$ ) as described by Schlichting [26]. All data compared is within the 'Full APG Region' as characterized by Brzek [6] and Anderson et al. [3] and [4]. ZPG smooth data from Osterlund [23] and ZPG rough data from Brzek [7] were also used for pressure gradient comparisons.

### Mean Profiles

The classical scaling failed to collapse the velocity profiles of Flows B and C into a single curve, where the flow is not in equilibrium according to the definition set forth by Clauser [14], as seen in Figure 5. The success observed by many investigators with this method on smooth/rough boundary layers is limited to ZPG flows. Therefore, in pressure gradient boundary layers this scaling will not collapse the data unless the external boundary layer is specifically designed to create a constant  $C_f$ , as in Clauser's equilibrium boundary layer. However, when

comparing smooth and rough profiles at a fixed streamwise location, the roughness effects are removed with only moderate deviations. These deviations, may be attributed to errors in  $u_*$  calculations. Therefore these results lean towards the results for smooth and rough ZPG flows of Schultz and Flack [28] and Brzek [7], where  $u_*$  is able to remove the effects of roughness. Figure 6 shows a comparison of rough APG and ZPG flows at a constant  $k^+$  for the classical scaling of the velocity deficit profile. Keeping a constant  $k^+$  value isolates the effect of pressure gradient. Here it is evident the impact that the APG has, where there is a dramatic increase of the APG profile over the entire boundary layer.

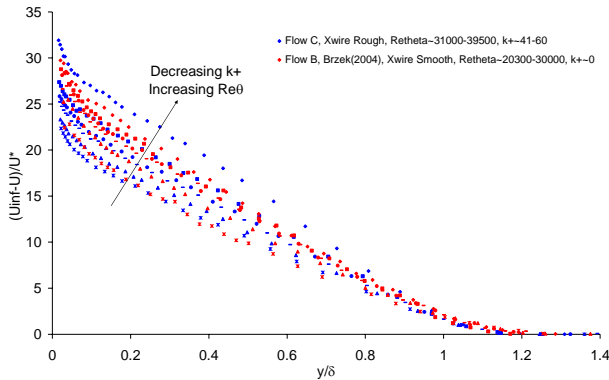


Figure 5. APG velocity deficit profiles, normalized by  $u_*$ , and  $\delta$ , for Flows B and C

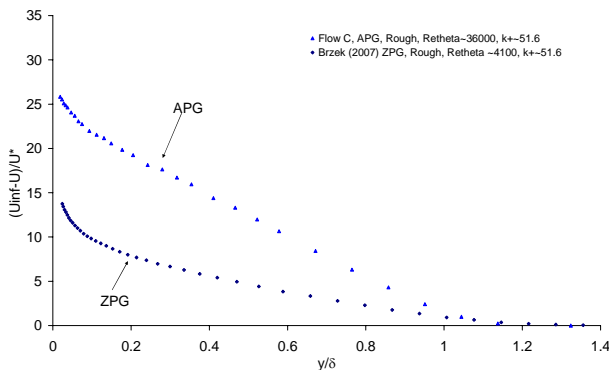


Figure 6. Rough APG and ZPG velocity deficit profiles, normalized by  $u_*$ , and  $\delta$ , at a constant  $k^+$

In Figure 7, the velocity deficit profiles of Flows B and C are normalized with the freestream velocity  $U_\infty$ , the Castillo and George [11] scaling. It is clear that the roughness effects of Flow C shift the profiles upwards from that of Flow B. This shift coincides with the smooth-rough ZPG comparisons of Brzek [7]. This plot also shows no evidence of data collapse or a sign of convergence to an asymptote as the Reynolds number approaches infinite, yet it illustrates two distinct regions for Flows B and C respectively. Therefore unlike the classical scaling, the Castillo and George [11] scaling does not show any signs of roughness dependence removal in the current APG configuration. In terms of pressure gradient effects, the Castillo and George [11] scaling has the similar results as the classical scaling where there is a dramatic increase of the APG profile over the entire boundary layer.

When the velocity deficit profiles of Flows B and C are normalized with the Zagarola and Smits scaling,  $U_\infty \delta^*/\delta$ , both Flows B and C collapse onto one curve in the outer region ( $y/\delta > 0.1$ ), Figure 8.

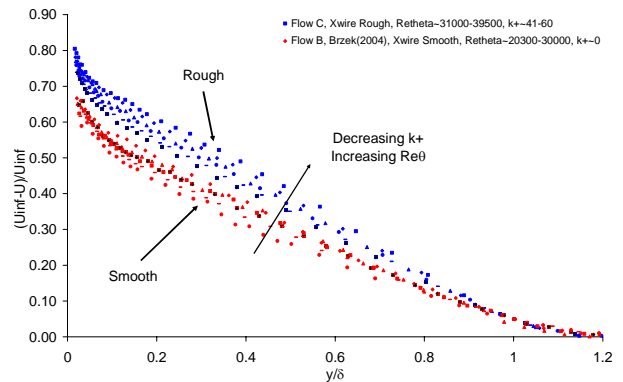


Figure 7. APG velocity deficit profiles, normalized by  $U_\infty$ , and  $\delta$ , for Flows B and C

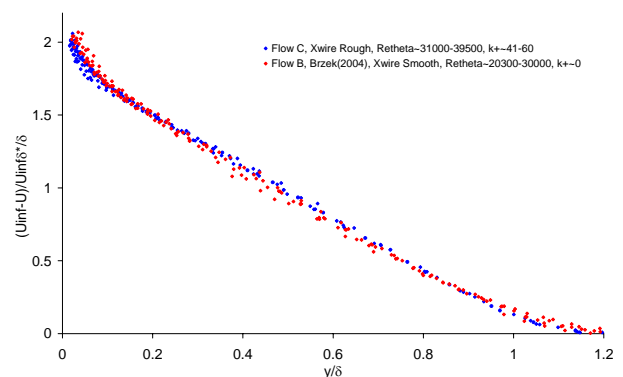


Figure 8. APG velocity deficit profiles, normalized with the Zagarola and Smits scaling,  $U_\infty \delta^*/\delta$  and  $\delta$ , of Flows B and C

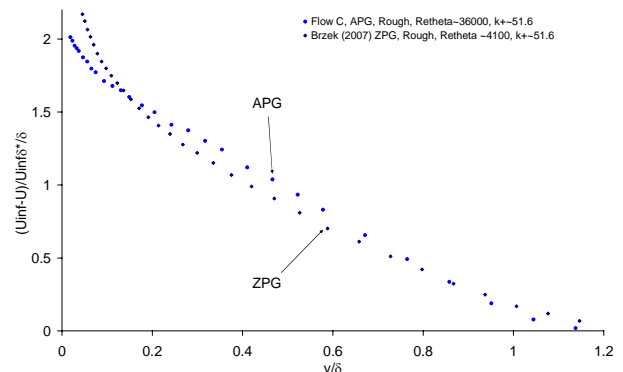


Figure 9. Rough APG and ZPG velocity deficit profiles, normalized with the Zagarola and Smits scaling,  $U_\infty \delta^*/\delta$  and  $\delta$  at a constant  $k^+$

The inner flow does not collapse nor is it independent of roughness effects. The effect of pressure gradient for this scaling between rough APG and ZPG flows is shown in Figure 9. Again as mentioned before, the data being compared is in the ‘Full APG Region’ of the test section, therefore a collapse of APG data is expected for similar surfaces. Both profiles fall into their corresponding pressure gradient bands as described by Walker and Castillo [32]. However, recent findings on high freestream turbulence experiments on ZPG and FPG (Brzek [7]) reveal that this scaling does not yield the success observed here. The current collapse of Flows B and C indicates that the Zagarola and Smits scaling removes the effects of roughness in the current APG flow configuration and that the Flow C data is indeed within the ‘Full APG Region’.

In Figure 10, the Reynolds normal stress,  $\langle u^2 \rangle$  shows removal of roughness effects using the classical scaling,  $u_*^2$ . Again the deviation in streamwise locations may be attributed to errors in  $u_*$ . As  $k^+$  decreases, the shift between profiles of same streamwise locations increases. The Reynolds normal stress,  $\langle v^2 \rangle$  was found to have similar effects as  $\langle u^2 \rangle$ , where there was a slight overall upward shift of Flow C due to roughness. However, at low Reynolds numbers, there is a clear Reynolds number dependence. This is interesting since Brzek [7] reports almost the opposite for their ZPG flow.

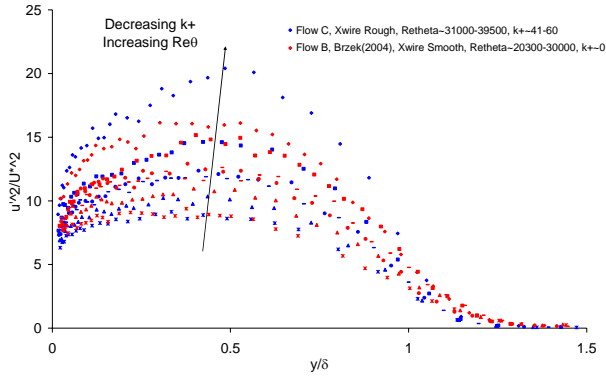


Figure 10. APG outer Reynolds normal stress  $\langle u^2 \rangle$  profile normalized using classical scaling,  $u_*^2$  and  $\delta$ , for Flows B and C

As for the Reynolds shear stress,  $\langle uv \rangle$ , there is heavy doubt on the accuracy of Flow B  $\langle uv \rangle$  data. This uncertainty in the  $\langle uv \rangle$  measurements in Flow B is attributed to an extreme imbalance of momentum in the inner region, where the only term in doubt is the  $\langle uv \rangle$  term. The imbalance can also be attributed to 3-dimensionality, yet the current Flow C  $\langle uv \rangle$  data maintained balance for a section of the inner region, therefore targeting the  $\langle uv \rangle$  term as the source of error in Flow B's imbalance. When  $\langle uv \rangle$  is scaled with  $u_*^2$ , two distinct bands for Flows B and C were found, where Flow C has a significant upward shift. The lack of collapse for smooth and rough indicates the importance of the pressure gradient for this non-equilibrium (Clauser [14]) APG flow. Furthermore, based on the doubt of the  $\langle uv \rangle$  data of Brzek [6], the effects of roughness cannot be compared for this component. Therefore, this investigation found the classical scaling only removes the effects of roughness for Reynolds normal stresses. Isolating the effects of pressure gradient by keeping a constant  $k^+$  value, Figure 11 illustrates a common trend for these variables and scaling, where there is a large increase from ZPG to APG.

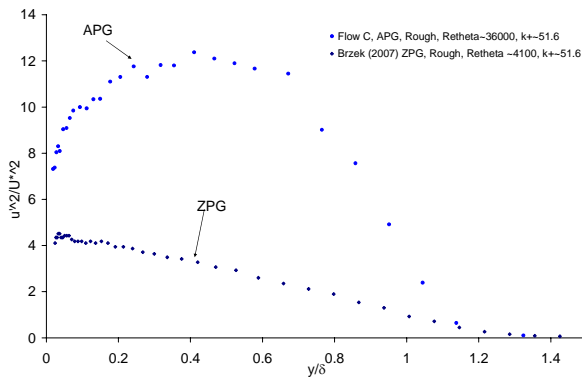


Figure 11. Rough APG and ZPG outer Reynolds normal stress  $\langle u^2 \rangle$  profile normalized using classical scaling,  $u_*^2$  and  $\delta$ , at a constant  $k^+$

In Figures 12 – 14, the Reynolds stress component profiles are normalized using the Castillo and George [11] scaling. This scaling uses  $U_\infty^2$  to scale the Reynolds normal stresses and

$U_\infty^2 d\delta/dx$  (boundary layer growth rate) to scale the Reynolds shear stress. All three Reynolds stress profiles show two distinct bands for Flows B and C, clearly identifying the significant impact of roughness. An interesting observation of the  $\langle v^2 \rangle$  profiles for Flow C is that before about  $0.3y/\delta$  the profiles collapse into a single curve. This indicates that the effects of pressure gradient are not as strong near the wall on this component. Thus,  $U_\infty$  contains more information about the pressure gradient, than information about roughness. This indicates that for flows with pressure gradient and roughness, a mixed scaling technique may be required. This was demonstrated in Brzek [7] with FPG roughness.

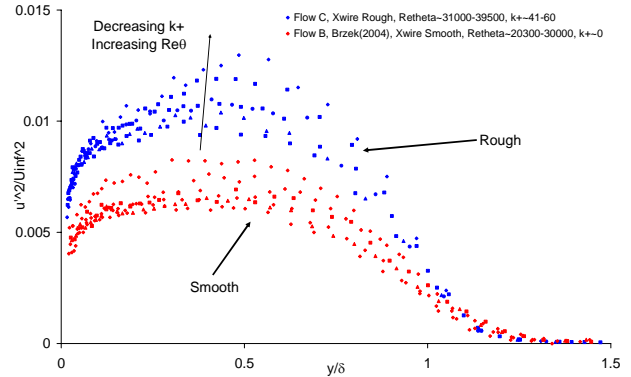


Figure 12. APG outer Reynolds normal stress  $\langle u^2 \rangle$  profile normalized by,  $U_\infty^2$  and  $\delta$ , for Flows B and C

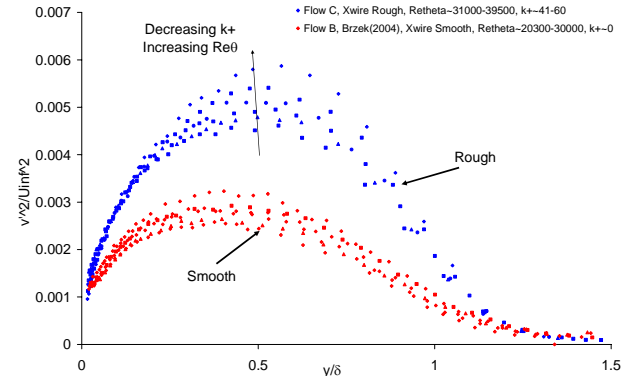


Figure 13. APG outer Reynolds normal stress  $\langle v^2 \rangle$  profile normalized by,  $U_\infty^2$  and  $\delta$ , for Flows B and C

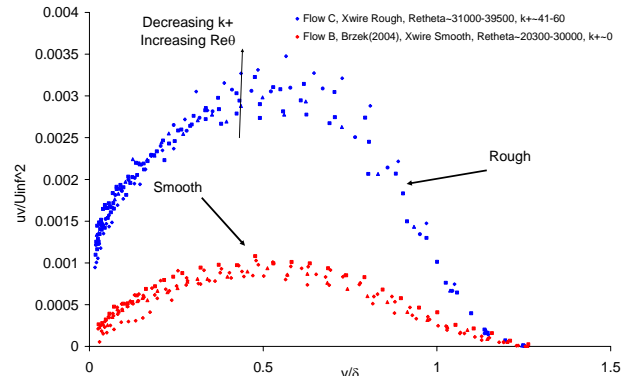


Figure 14. APG outer Reynolds shear stress  $\langle uv \rangle$  profile normalized using by,  $U_\infty^2 d\delta/dx$ , and  $\delta$ , for Flows B and C

Figure 15 illustrates the effects of pressure gradient on the Reynolds normal stress,  $\langle u^2 \rangle$  component profile ( $\langle v^2 \rangle$  has similar trend), which is normalized using the Castillo and George [11] scaling. This pressure gradient isolation illustrates that the normal stress profiles for ZPG have different profile trends than APG, yet they have similar magnitudes. When scaling the

Reynolds shear stress,  $\langle uv \rangle$  with Castillo and George [11] scaling, the profile for ZPG is much higher than APG, due to the larger boundary layer growth rate, Figure 16.

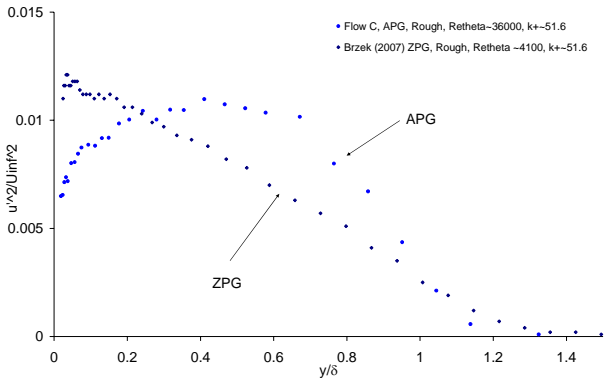


Figure 15. Rough APG and ZPG outer Reynolds normal stress  $\langle u'^2 \rangle$  profile normalized by,  $U_\infty^2$  and  $\delta$ , at a constant  $k^+$

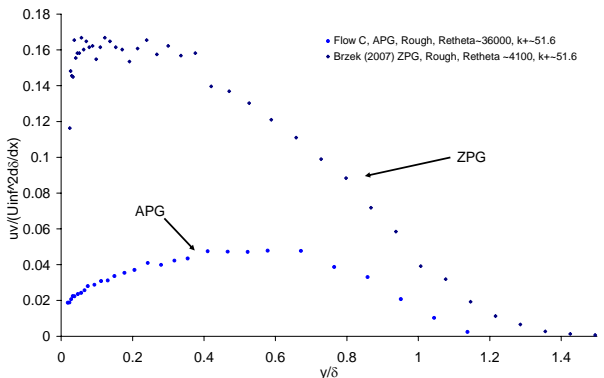


Figure 16. Rough APG and ZPG outer Reynolds shear stress  $\langle uv \rangle$  profile normalized by,  $U_\infty^2 d\delta/dx$ , and  $\delta$ , at a constant  $k^+$

The inner mean velocity profiles normalized by  $u_*$  and  $v/u_*$ , for Flows B and C are shown in Figure 17. This figure clearly indicates the strong effects of roughness to Flow C. As  $k^+$  increases, the profiles shift downward due to the increase in friction velocity. In the case of Flow C, since it is an APG flow, the friction velocity decreases with streamwise progression and the influence of the roughness decreases. Thus, profiles move slightly towards the smooth profile even though the Reynolds number is increasing.

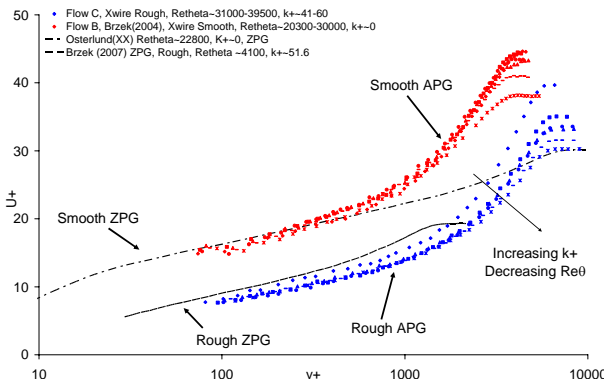


Figure 17. Inner mean velocity profiles normalized by  $u_*$  and  $v/u_*$ , for APG Flows B and C, Smooth ZPG Osterlund (1999), and Rough ZPG Brzek [7]

The classical theory and similarity analysis of George and Castillo [16] both suggest normalizing the inner Reynolds Stress profiles with the friction velocity,  $u_*^2$ , as shown in Figures 18 -

20. It is apparent in all three component profiles that there is a Reynolds number and roughness dependence. The inner region and up to about  $0.2y/\delta$  of the  $\langle u'^2 \rangle$  profiles seem to show roughness independence, yet the Reynolds number effect is evident. It is also found that in the inner region, the  $\langle v'^2 \rangle$  profile does not show a significant effect of roughness as seen in the ZPG data of Brzek [7]. As for  $\langle uv \rangle$  there are two distinct bands present in the  $\langle uv \rangle$  profiles relative to Flows B and C, where

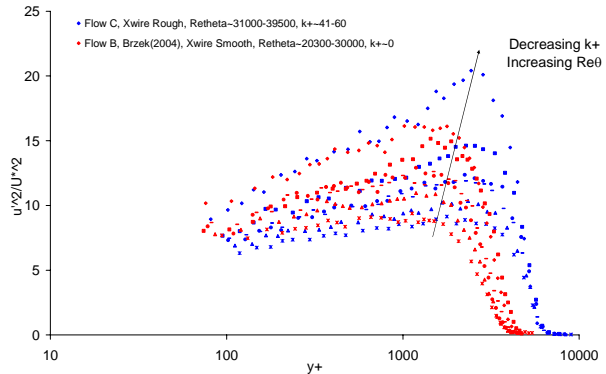


Figure 18. APG inner Reynolds normal stress  $\langle u'^2 \rangle$  profiles normalized by  $u_*^2$  and  $v/u_*$ , for Flows B and C

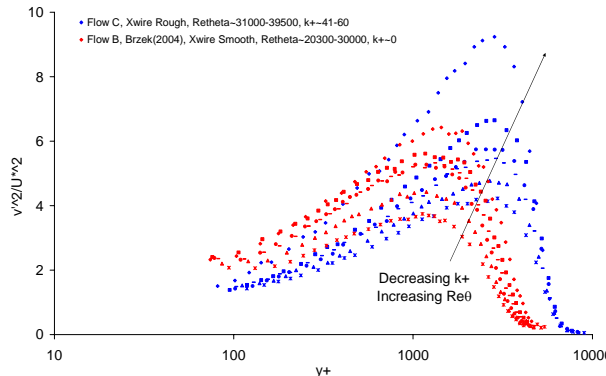


Figure 19. APG inner Reynolds normal stress  $\langle v'^2 \rangle$  profiles normalized by  $u_*^2$  and  $v/u_*$ , for Flows B and C

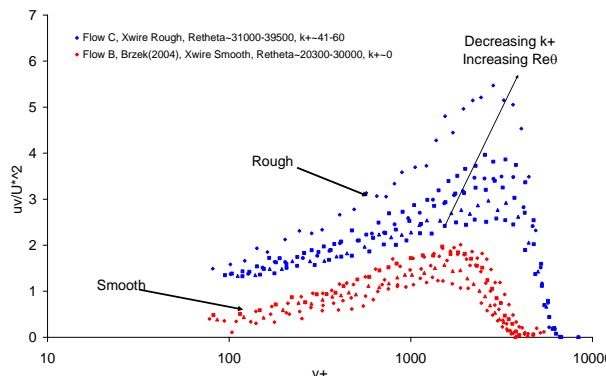


Figure 20. APG inner Reynolds shear stress  $\langle uv \rangle$  profiles normalized by  $u_*^2$  and  $v/u_*$ , for Flows B and C Flow C's roughness effect is evident. As mentioned above there is high uncertainty of the validity of the  $\langle uv \rangle$  comparison for Flow B.

### Conclusions

The main goal of this experimental investigation has been to isolate the effects of surface roughness in adverse pressure gradient turbulent boundary layer flows. This isolation of roughness effects was successfully carried out by changing only the roughness variable and keeping all other experimental

conditions constant (i.e.  $T_\infty$ ,  $U_{ref}$ , and  $C_p$ ). ZPG smooth data from Osterlund [23] and ZPG rough data from Brzek [7] were also used for pressure gradient comparisons.

In the comparisons of smooth (Flow B,  $Re_\theta=20,300-30,000$ ,  $k^+=0$ , finely sanded particle board) and rough (Flow C,  $Re_\theta=31,000-39,500$ ,  $k^+=41-60$ , 24-grit sand paper) data, it was found that the mean velocity near the wall was significantly reduced for Flow C. Various scalings were explored and used for comparisons of the smooth and rough mean velocity and Reynolds stress profiles. The classical scaling removed roughness effects for the outer mean velocity and Reynolds normal stresses, where minimal deviations may be attributed to error in measurements or the derivation of  $u^*$ . The velocity profiles in inner variables show a downward shift due to roughness. When the velocity and Reynolds stress profiles were scaled with  $U_\infty$ , all results showed a clear roughness effect as an upward shift or increase in profiles. More importantly the Zagarola and Smits scaling successfully collapsed all rough and smooth APG data in the outer region.

The study also included the effects of pressure gradients between ZPG and APG flows by fixing the roughness parameter. When a fixed roughness was observed, it was apparent in the Zagarola and Smits scaling of the velocity profiles, that Flow C did indeed fall into the ‘Full APG Region’ described by Brzek [6]. All profiles for the outer velocity and Reynolds stresses normalized with  $u^*$  along with the outer velocity profiles scaled with  $U_\infty$  showed a significant increase in profiles due to APG. Another important observation is that the outer Reynolds normal stresses scaled with  $U_\infty$  showed different profile trends with similar magnitudes for ZPG and APG flows.

*Due to lack of space, the current findings of boundary layer parameters and the pressure parameter  $\Lambda$  have been excluded from this paper. These points will be discussed during the presentation.*

### Acknowledgments

This work was carried out while the first author was on leave from Rensselaer Polytechnic Institute at Victoria University during the course of his Masters degree program. A special thanks to Victoria University and Dr. Turan for the use of their facility and Dr. Roosevelt Johnson from NSF-AGEP for making this international collaboration possible. Also a special thanks to Catherine Anderson and Brian Brzek for their extensive contributions and guidance throughout this project.

### References

[1] Akinlade, O. G., Bergstrom, D. J., Tachie, M. F., and Castillo, L., *Outer flow scaling of smooth and rough wall turbulent boundary layers*, Exp. Fluids, Vol. 37, pp. 604-612, 2004

[2] Anderson, C., PhD Thesis in progress, Victoria University, 2007.

[3] Anderson, C., Turan, Ö.F., Brzek, B. and Castillo, L., *Adverse pressure gradient turbulent boundary layer flows, Part 1: Flow development*, AFMC, Sydney, NSW. AFMC15-259. F, 2004

[4] Anderson, C., Turan, Ö.F., Brzek, B. and Castillo, L., *Adverse pressure gradient turbulent boundary layer flows, Part 2: Scaling of Reynolds stresses*, AFMC, Sydney, NSW. AFMC15-260. F, 2004

[5] Bergstrom, D. J., *The effects of surface roughness on the mean velocity profile in a turbulent boundary layer*, ASME, Vol. 124, pp. 664-670, 2002.

[6] Brzek, B., *Development and characterization of an increasing adverse pressure gradient turbulent boundary layer*, Master’s Thesis, Rensselaer Polytechnic Institute, 2004.

[7] Brzek, B., *The effects of external conditions in turbulent boundary layers*, PhD Thesis, Rensselaer Polytechnic Institute, 2007

[8] Brzek, B., Cal, R. B., *LDA Measurements in rough surface ZPG turbulent boundary layers*, FEDSM2006-98508, 2006.

[9] Cal, R., *The favorable pressure gradient*, PhD thesis, Rensselaer Polytechnic Institute, 2006.

[10] Castillo, L., *application of Zagarola/Smits scaling in turbulent boundary layers with pressure gradient*, Advances in Fluid Mechanics III, AFM 2000:275-288, 2001.

[11] Castillo, L., and George, W. K., *Similarity analysis for turbulent boundary layer with pressure gradient: outer flow*, AIAA Journal, Vol. 39, No. 1, pp. 41-47, 2001.

[12] Castillo, L., Seo, J., Hangan, H., and Johansson, T., *Smooth and rough turbulent boundary layers at high Reynolds number*, Exp. in Fluids, Vol. 36, pp. 759-774, 2004.

[13] Chao, D., *Turbulence measurements in an APG boundary layer*, Rensselaer Polytechnic Institute, Senior Undergraduate Project, 2004.

[14] Clauser, F., *Turbulent boundary layers*, Adv. Applied Mech., Vol. 4, pp. 1-51, 1954.

[15] Clauser, F. H., *Turbulent boundary layers in adverse pressure gradients*, AIAA Journal Special Supplement: Centennial of Powered Flight, pp. 238-255, 1953.

[16] George, W., and Castillo, L., *Zero-pressure-gradient turbulent boundary layer*, Appl. Mech. Rev., Vol. 50, No. 12, pp. 689-728, 1997.

[17] George, W. K., *Some new ideas for similarity of turbulent shear flows*, Turbulence, Heat and Mass Transfer, Lisbon, 1004, edited by K. Hanjalic and J.C.F. Pereira, Begell House, New York, pp. 24-49, 1995.

[18] Krogstad, P. A., and Antonia R. A., *Surface roughness effects in turbulent boundary layers*, Exp. Fluids, Vol. 27, pp. 450-460, 1999.

[19] Krogstad, P. A., and Antonia R. A., *Turbulence structure in boundary layers over different types of surface roughness*, Fluid Dynamics Research, Vol. 28, pp. 139-157, 2001.

[20] Ludwig, H., and Tillmann, W., *Investigations of the wall shearing stress in turbulent boundary layers*, NACA TM, No. 1285, 1950.

[21] Lueptow, R. M., *Computer-aided calibration of X-probes using a look-up table*, Exp. in Fluids, Vol. 6, pp. 115-118, 1988

[22] Newhall, K., *Turbulent boundary layers: a look at skin friction, pressure gradient, surface roughness and the power law*, Master’s Thesis, Rensselaer Polytechnic Institute, 2006.

[23] Osterlund, J., *Experimental studies of zero pressure-gradient turbulent boundary layer flow*, PhD Thesis, KTH, Stockholm, Sweden, 1999.

[24] Perry, A. E., and Joubert, P. N., *Rough-wall boundary layers in adverse pressure gradients*, J. Fluid Mech., Vol. 17, pp. 193-211, 1963

[25] Perry, A. E., Schofield, W. H., and Joubert P. N., *Rough wall turbulent boundary layers*, Fluid Mech., Vol. 37, pp. 383-413, 1969.

[26] Schlichting, H., *Boundary layer theory*, Seventh edition, McGraw-Hill, 1979.

[27] Schubauer, G. B., and Klenamoff, P. S., *Investigation of separation of the turbulent boundary layer*, NACA TN, No. 2133, 1950.

[28] Schultz, M., and Flack, K., *Turbulent boundary layers over surfaces smoothed by sanding*, J. Fluids Eng., Vol. 125, pp. 863-870, 2003.

[29] Seo, J., *Investigation of upstream conditions and surface roughness in turbulent boundary layer*, PhD Thesis, Rensselaer Polytechnic Institute, 2003.

[30] Tachie, M. F., Bergstrom, D. J., and Balachandar, R., *Rough wall turbulent boundary layers in shallow open channel flow*, ASME J. Fluids Eng., Vol. 122, pp. 533-541, 2000.

[31] Tachie, M. F., Bergstrom, D. J., and Balachandar, R., *Roughness effects in low-Reynolds numbers open channel turbulent boundary layers*, Exp. Fluids, Vol. 35, pp. 338-346, 2003.

[32] Walker, D. and Castillo, L., *The effects of the upstream conditions on turbulent boundary layers*, AIAA Journal, Vol. 40 No. 12, pp. 2540-2542, 2002.

[33] Wang, X., *Similarity analysis for turbulent boundary layers subject to pressure gradient and heat transfer*, PhD Thesis, Rensselaer Polytechnic Institute, 2003.

[34] Zagarola, M., and Smits, A., *A new mean velocity scaling for turbulent boundary layers*, Proceedings of FEDSM’98, Washington D.C., 1998b

[35] Zagarola, M., and Smits, A., *Mean-flow scaling of turbulent pipe flow*, J. Fluid Mech., Vol. 373, pp. 33-79, 1998